Oil-Jet Lubrication of Epicyclic Gear Trains

Matthias Haber, Corina Schwitzke, Hans-Jörg Bauer
Institut für Thermische Strömungsmaschinen
Karlsruhe Institute of Technology (KIT)
Karlsruhe, Germany
haber@kit.edu

Abstract—**Predicting and understanding the evolving oil distribution is the major key for the design of efficient and reliable cooling and lubrication systems in gear boxes. The complexity of multiple rotating and moving parts and the bad accessibility necessitate costly and complicated experimental approaches. Suitable numerical simulation methods promise to overcome the given experimental limitations.**

In this work the oil-jet lubrication in an epicyclic gear train with fixed carrier frame and a transmission ratio of $1 : 2.95$ is investigated. From a modelling perspective the main challenges are in the heavily deforming computational domains, accurate and sharp representation of the oil surface, high temporal and spatial resolutions and computational efficiency on parallel architectures. Hence, a single phase "free surface" Smoothed Particle Hydrodynamics approach was chosen as the most suitable. The study is conducted for two different positions of the nozzle. To capture three-dimensional effects of the oil flow, the simulations were setup in 3D. The resulting oil distributions are presented and phenomenologically discussed. Especially the influence of different nozzle positions on the oil distribution near the gear meshing is compared and highlighted.

I. Introduction

Epicyclic gear trains are widely used as reduction transmissions because of their high power density for example in the fields of automotive applications, power generation and aeronautics. Especially highest power density transmissions need sophisticated cooling and lubrication strategies. A common solution for high-speed gears is the oil-jet lubrication. Oil is fed through nozzles, directed in jets either onto the gears and impinges on them or into the gear meshing. Understanding the distribution of the oil and its interaction with the gears is crucial for design and optimization of these systems. Hence, investigation and understanding of the evolving two-phase flow play the key role in correctly predicting cooling and lubrication processes.

In the last century oil-jet lubrication was mainly investigated experimentally due to the available comparatively low computational power. Major contributions originate from Akin et al. [1] and Handschuh [2]. In the last years experiments to determine the heat transfer on a single gear with oil-jet cooling were conducted by Ayan et al. ([3], [4]) and von Plehwe [5]. Nevertheless numerical methods are essential to open detailed insights to the flow phenomena in a gear train. Fondelli et al. [6] and Yazdani and Soteriou [7] used the Volume-of-Fluid (VOF) method with adaptive mesh refinement for numerical studies in this field. Smoothed Particle Hydrodynamics (SPH) simulations were conducted by Mettichi et al. [8] for a whole gearbox with lower resolution than targeted in the present work. Keller worked a lot on simulation methodologies for oil-jet lubrication of gears. Keller et al. [9] compared VOF simulations and two phase SPH simulations by studying the wetting behaviour and impingement depth for a single gear. Later ([10]–[13]) the framework was extended to the "free surface" single phase SPH (SPSPH) approach and sophisticated post processing strategies as well as parameter studies presented. These studies were mainly conducted on a generic single gear geomtery. The simulation tools were employed on two meshing external spur gears and proofed the capability of the developed methodology to model meshing gears in [14].

II. Methodology

From a modelling perspective the main challenges for the numerical method of choice are firstly an accurate and sharp representation of the oil surface, which is a general requirement for two-phase flows, and secondly the heavily deforming computational domain due to the interlocking gears. Additionally the method needs to grant high computational efficiency on parallel architectures to achieve acceptable wall clock times despite of the immense required computational effort. Based on the work of Keller [14] the single phase "free surface" SPH approach is selected as the most suitable method. The basic formulation and used models are presented hereinafter.

At the "Institut für Thermische Strömungsmaschinen" (ITS) a highly parallelized weakly-compressible SPH code (turboSPH) is developed [15]. In the last decade the code was employed on various engineering applications like fuel atomization ([16],[17]), oil film dynamics in an aero engine bearing chamber ([18],[19]), gear lubrication ([9], [13]), falling wall film reactors ([20]), homogenizers [21] and has proofed its wide range applicability to scientific and industrial problems. Assuming an isothermal flow, the purely Lagrangian SPH formulation of the discretized Navier-Stokes equations is stated as:

$$\left\langle \frac{D\rho}{Dt} \right\rangle_a = \sum_b m_b \vec{u}_{ab} \cdot \vec{\nabla} W_{ab,h} \qquad (1)$$

$$\left\langle \frac{D\vec{u}}{Dt} \right\rangle_a = \left\langle -\frac{\vec{\nabla} p}{\rho} \right\rangle_a + \left\langle \frac{\vec{\nabla} \cdot \mathbf{S}}{\rho} \right\rangle_a + \left\langle \vec{f}_\sigma \right\rangle_a \qquad (2)$$

$$\Delta p_a = \frac{c_a^2 \rho_{0,a}}{\gamma_a} \left[\left(\frac{\rho_a}{\rho_{0,a}} \right)^{\gamma_a} - 1 \right] \qquad (3)$$

The temporal variation in density ρ of a particle a is expressed in equation (1) by the standard SPH approximation of the mass continuity equation. It is calculated by evaluating the velocity differences $\vec{u}_{ab}$ of the particle a to its neighbouring particles b within the sphere of influence and weighting them with the kernel gradient $\vec{\nabla} W_{ab,h}$. The quantity m describes the mass of the particle. Equation (2) states the momentum equation. On the LHS, the acceleration of the particle a is given. The RHS represents the acting forces on the particle, that lead to the acceleration. They can be caused by pressure gradients, by shear stresses, by surface tension or any other external body forces like gravity. The latter is not considered in this work. The pressure gradient is calculated with the locally conservative form, proposed by Colagrossi and Landrin [22]. Viscous shear stresses are modeled with the approach from Szewc et al. [23]. Surface tension is considered by the continuum surface force (CSF) model, that was introduced by Adami et al. [24] and adapted by Wieth at al. [25]. To close the equation system, the pressure p_a is directly calculated from the density in equation (3). Therefore a reference density $\rho_{0,a}$ is defined. γ_a is the polytropic exponent and is usually set to 7 for liquids. In order to minimize density fluctuations below 1%, the artificial speed of sound should be chosen to approximately 10 times the global $||\vec{u}_{max}||$. This kind of closure is known as weakly compressible SPH (WCSPH).

In this work the SPSPH approach is used. The idea is to model two-phase flows of high density ratios and low momentum exchange from phase to phase by neglecting the sparse phase and modeling the dense phase. Specifically, the oil phase is discretized with fluid particles, the air volume is void. Equation (1) is highly suitable to avoid density diffusion at the free surfaces but it does not ensure full mass conservation. This drawback has to be compensated by periodic re-initialisation of the density field. The so-called Shepard-Filter [27] is applied. More information can be found in the work of Randles and Libersky[28].

The implemented boundary conditions are elaborated by Braun et al. [29]. Walls have to be modeled by sufficient number of layers of wall particles to cover the whole sphere of influence of a fluid particle in vicinity to the wall. Permeable boundary conditions, which are inlet, outlet and periodic boundary conditions, are indicated by marker particles. The time integration is performed by an explicit predictor-corrector scheme, with an adaptive CFL-criteria based time stepping.

Main characteristics of the investigated oil-jet lubrication system are the rotational movements of the gear solid bodies.
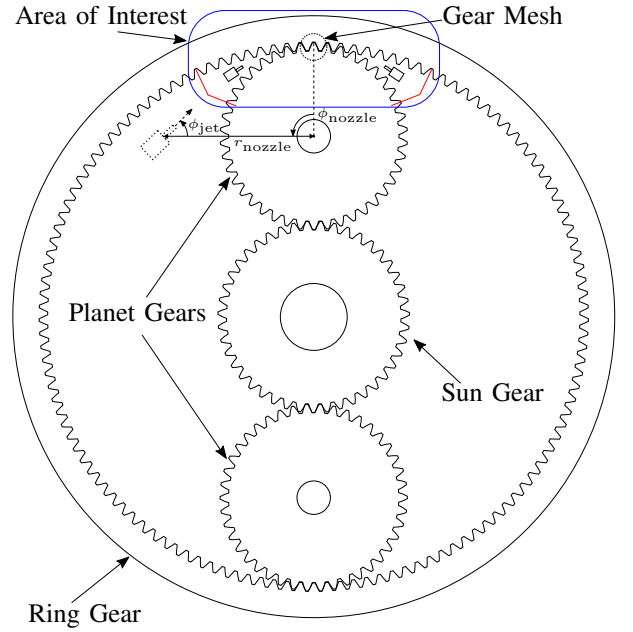

Fig. 1.   Geometry of the Setup

These are incorporated by prescribing the angular velocities and center of rotations of the bodies. During execution of the simulation the positions and velocities of every solid body particle are calculated and updated timestep-wise.

III. NUMERICAL SETUP

Goal of the numerical simulations is the prediction of the oil distribution for oil-jet lubrication in a epicyclic gear train. Heat transfer is not modeled. In Figure 1 the investigated geometry is sketched. Epicyclic gear trains comprise of a sun gear in the centre, planet gears, which are arranged circumferential to the sun supported by the carrier, and the ring gear, which is an internal gear. In an oil-jet lubrication oil is fed through a nozzle onto the gears. This leads to an intermittent impingement of the oil on the gear flanks. In the following sections the geometry, kinematics, boundary conditions, operating conditions and SPSPH-inherent choice of numerical parameters are explained.

A. Geometry

An epicyclic gear train with a fixed carrier frame and transmission ratio of approximately $1 : 2.95$ is investigated. For cooling and lubrication purposes a static nozzle, that is located in vicinity to the gear mesh of the ring gear and a planet gear, injects oil onto the gear flanks. The internal and the external gear are designed as spur gears with involute profiles. The geometry and kinematics are chosen in accordance with DIN ISO 21771 [26]. No profile shifting is considered. All geometric information is listed in table I.

To reduce the computational effort, circumferential segments of the ring gear and the planet gear are extracted. The sun gear in the center of the gear box is not considered because the interaction of the oil with the teeth in proximity of the

TABLE I
GEOMETRICAL PROPERTIES OF THE MODELED GEAR TRAIN

Property	Symbol	Value
Jet Diameter	D_{jet}	$1\,D_{\text{jet}}$
Inlet Duct Length	L_{inlet}	$1\,D_{\text{jet}}$
Module	m	$4\,D_{\text{jet}}$
Pitch Diameter Ring	$D_{\text{p,Ring}}$	$508\,D_{\text{jet}}$
Number of Teeth Ring	z_{Ring}	127
Pitch Diameter Planet	$D_{\text{p,Planet}}$	$168\,D_{\text{jet}}$
Number of Teeth Planet	z_{Planet}	42
Gear Width (Ring and Planet)	L_{width}	$15\,D_{\text{jet}}$
Pressure Angle	α	$25°$
Addendum Modification Coefficient	x	0
Number of Teeth Ring Segment	$z_{\text{S,Ring}}$	18
Number of Teeth Planet Segment	$z_{\text{S,Planet}}$	16
Nozzle Position Radial	r_{nozzle}	$91.7\,D_{\text{jet}}$
Nozzle Position Angular	ϕ_{nozzle}	$\pm 29.8°$
Angular Jet Direction	ϕ_{jet}	$\pm 79°$

TABLE II
BOUNDARY CONDITIONS AND KINEMATICS

Property	Symbol	Value
Angular Velocity Ring	ω_{Ring}	$168.83\,\text{s}^{-1}$
Angular Velocity Planet	ω_{Planet}	$510.51\,\text{s}^{-1}$
Rotational Speed Ring	n_{Ring}	$1612\,\text{min}^{-1}$
Rotational Speed Planet	n_{Planet}	$4875\,\text{min}^{-1}$
Bulk Velocity Nozzle Inlet	$v_{\text{B,nozzle}}$	$33.14\,\text{m}\,\text{s}^{-1}$

TABLE III
FLUID PROPERTIES AT $80\,°\text{C}$ AND $101\,325\,\text{Pa}$

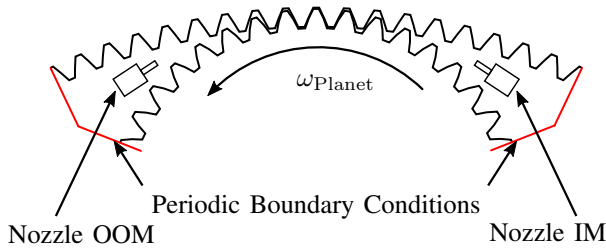| Property	Oil	Air
Density ρ in $\text{kg}\,\text{m}^{-3}$	949	0.9862
Dynamic Viscosity μ in $\text{Pa}\,\text{s}$	7.90×10^{-3}	21.01×10^{-6}
Surface Tension σ in $\text{N}\,\text{m}^{-1}$	0.025	
Contact Angle (Oil-Wall) θ in $°$	45	

Fig. 2.   Computational Domain

gear meshing of planet and ring gear is in the focus of this study. This region is indicated as Area of Interest in Figure 1. The extraction leads to the geometry shown in figure 2. The distribution of the oil film during and after the impingement process involves laterally varying velocity components on the gear flanks. Therefore, the whole setup has to be considered three-dimensional.

B. Boundary Conditions

The extracted segment is confined radially by the teeth of the ring gear and the planet gear. Those walls are modelled with three layers of wall particles to grant full kernel support for fluid particles in wall proximity. The rotational solid body movement of the gears is prescribed accordingly to table II. The marker particles for the rotational periodic boundary conditions terminate the domain in angular direction. As depicted in Figure 2 the marker particles originate purely radially from the ring gear and the planet gear respectively. Their intersection is located at half the distance between the ring gear and the planet gear. In lateral direction the domain is bounded by an outlet condition, that basically deletes particles, if they cross it.

The oil is injected through a simplified generic nozzle of cylindrical shape. The inlet is placed in the duct of the nozzle upstream the nozzle exit. Two different nozzle configurations

are investigated within this work. The first position is called "Into Meshing" (IM), where the oil-jet is directed towards the gear meshing nearly parallel to the circumferential velocity component of the rotating gears. The second position is axisymmetric to the first (IM) and is called "Out Of Meshing" (OOM). The oil-jet is directed in opposite direction against the circumferential velocity component of the rotating gears. The exact positions are given in table II. For both cases (IM and OOM) the direction of the oil-jet is chosen to ensure the longest possible undisturbed penetration into the narrowing gap between ring gear and planet gear.

C. Operating Conditions

The investigations are conducted with the fluid properties of Mobil Jet Oil II at a temperature of $80\,°\text{C}$, which is a typical steady-state oil temperature in gear boxes. Changes of its properties due to local heating of the oil are not considered. Even though the air is not discretized, their fluid properties are necessary in order to calculate the surface tension forces on the oil. For the sake of completeness material properties of both fluids are presented in Table III.

D. Numerical Parameters

The mean particle spacing is $\Delta x = 0.05\,D_{\text{jet}}$. As kernel function a quintic spline is chosen with a smoothing length of $h = \Delta x$ and a maximum radius of influence of $r_{max} = 3h$. This leads to an initial particle count of 14.4×10^6 particles. The number increases during simulation, because oil is injected and distributed in the domain. The artificial speed of sound is set to $c = 500\,\text{m}\,\text{s}^{-1}$. The convective flow CFL number is set to 0.3 resulting in a time step of approximately $2.5 \times 10^{-8}\,\text{s}$. Data is written with a frequency of $f_{save} = 200\,\text{kHz}$. The density field is reassigned every $N_{\text{Shepard}} = 5$ time steps with a upper limit for tolerated density fluctuations of 0.5%.

Fig. 3.   Oil Distribution at $t^+ \approx 9$ (IM)

IV. RESULTS

Figure 3 shows the complex three-dimensional oil distribution at a dimensionless time of $t^+ \approx 9$ for the case IM. The dimensionless time is defined as $t^+ = {tz\omega}/{2\pi}$, where t represents the physikal time, ω is the angular velocity and z stands for the number of teeth of a gear. Illustratively, it can be seen as the number of teeth that passed a certain point on the circumference since the start of the simulation. Every oil particle is drawn as a small sphere of diameter Δx.

To identify different encountered phenomena and for comparison the resulting oil distributions are presented hereinafter from a purely two dimensional axial perspective. Figure 4 shows the evolving oil distribution of the IM configuration for five subsequent time steps. The dimensionless time t_i^+ is defined analogously to t^+ but shifted, that the time $t_i^+ = 0$ marks the beginning of the impingement of the oil-jet on the next nonwetted tooth of the planet gear. Due to the intermittent characteristics of the process, all phenomena repeat periodically for the subsequent tooth at a dimensionless time $t_i^+ = 1$.

At $t_i^+ = 0$ the oil-jet slightly touches the top land of tooth T_1 of the planet gear. Until $t_i^+ = 0.2$ the top land of T_1 dives fully into the jet and marginally deflects the jet radially outwards. On the leading flank of the tooth the oil-jet starts to widen and builds up a film that is moving towards the root of T_1. The circumferential velocity of the planet gear is a bit higher than the tangential component of the jet velocity. Thus, T_1 can be observed overtaking the oil-jet in the subsequently presented time steps. From $t_i^+ = 0.4$ on a gap on the trailing flank of T_1 begins to open up. Due to the existing contact with the gear top land the jet is stretched in that gap region. At the leading flank the still cylindrically shaped segment of the jet is shortened and feeds the forming film on this flank. In the next time steps ($t_i^+ = 0.6$, $t_i^+ = 0.8$) it can be seen how the already deflected segments of the jet disintegrate more and more because of the impingement processes. The oil spreads increasingly lateral. Centrifugal forces strip the films radially outwards from the planet gear (cf. leading flank T_2 at $t_i^+ = 0.8$). Most of this oil is caught by the ring gear and transported on the wetted teeth towards the gear meshing and as a thin film through it. A few moments later than $t_i^+ = 0.8$ the succeeding tooth of T_1 on the ring gear hits the undisturbed oil-jet. That is the only observable direct interaction of the ring gear with the jet. Later wetting of the ring gear is mainly driven
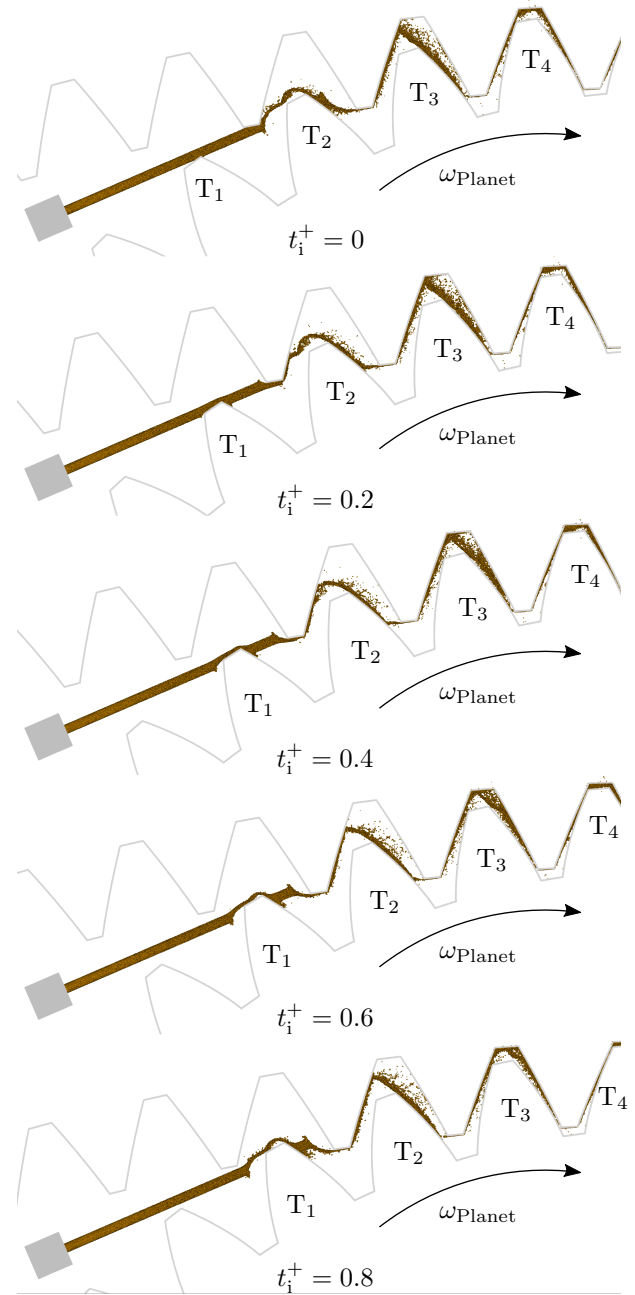

Fig. 4.   Temporal Evolution of Oil Distribution (IM) 2D

by centrifugal forces or the tremendously narrowing gap with between ring gear and planet gear. For $t_i^+ = 1$ all described phenomena start again for the following teeth.

In the next paragraph the OOM configuration is presented in the same way. Figure 5 shows the evolution of the oil distribution for five different time steps. The time $t_i^+ = 0$ marks the first contact of a nonwetted tooth of the planet gear. The biggest difference of the OOM to the IM configuration lays in the high relative velocity between oil-jet and the circumferential velocities of the gears. The resulting impact accelerations on the oil during the impingement processes are
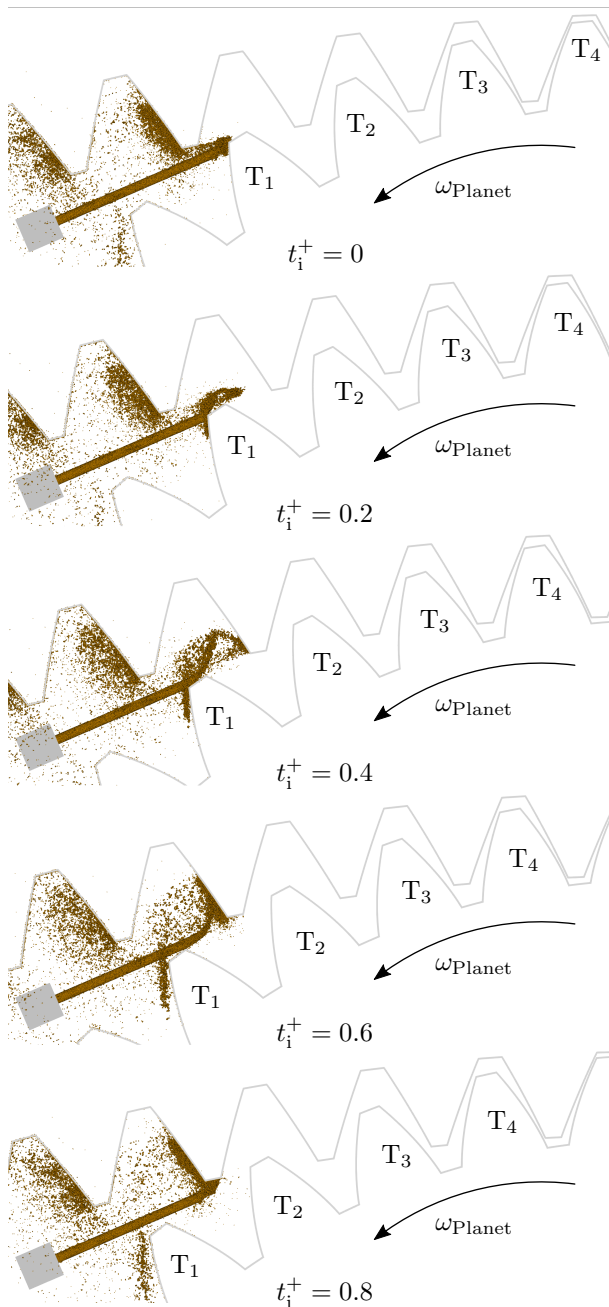
Fig. 5.   Temporal Evolution of Oil Distribution (OOM) 2D

is the closest position to the meshing, that can be directly wetted by a significant amount of oil. Indirect wetting by a full revolution of oil sticking to a gear flank is not considered in this work. For $t_i^+ = 0.6$ and later the jet starts to separate from the top land of T_1. Also the film resulting from the part of oil, that was directed towards the root, cannot resist the centrifugal forces anymore and starts to separate from the leading flank of T_1.

Apparently the OOM configuration does not yield any direct lubrication of the gear meshing. From a design point of view the IM configuration is much more promising, because it ensures that the oil film is fed into the gear meshing.

Additionally, to get an idea of the lateral oil distribution the three-dimensional renderings are compared within the figures 6 and 7. The necessity to use three-dimensional se-tups becomes obvious for both configurations because of the inhomogeneous lateral oil distribution. In both cases the oil is spread axially, after the the impingements on the teeth. Additionally, in the IM configuration the squeezing in the narrow gap near the gear meshing deflects the oil axial, too. The IM configuration catches and collects a lot of oil in the root regions of the ring gear. On the one hand this accumulation results from the centrifugal forces, pushing the oil radially outwards, on the other hand it is enforced by the geometry itself. In the root region the height of the gap between ring gear and planet gear is wider than at the flanks, where direct contact of the flanks occurs. The contact pressure at the flanks squeezes the oil. It flows towards regions of lower contact pressure. Thus it escapes partially in axial direction as well as towards areas of wider gap heights. As seen in 2D, the OOM configuration does not provide direct lubrication to the meshing. Additionally the wetted area is obviously higher for the IM configuration. This leads to a better lubrication and heat transfer for cooling.

Both cases reveal, that a higher resolution would be desir-able in order to resolve the forming oil films more accurate. Nevertheless the chosen resolution provides a compromise of accuracy and computational effort, which is approximately 4×10^4 CPUh per simulation.

much more violent. This is noticeable at a first glance in figure 5 by the huge forming particle clouds. For comparison the image sections are exactly the same as in figure 4. At $t_i^+ = 0$ the oil-jet impinges on the leading flank of tooth T_1 of the planet gear. While flowing over the top land of T_1 deflection in radially outward direction of a major part of the oil is initiated (cf. $t_i^+ = 0.2$). At the same time the jet is split by the leading flank tip. The smaller part is guided towards the root of tooth T_1. In the next time step $t_i^+ = 0.4$ the radially outward deflected oil already reaches the leading flank of the precursive tooth of the ring gear (between T_1 and T_2). That
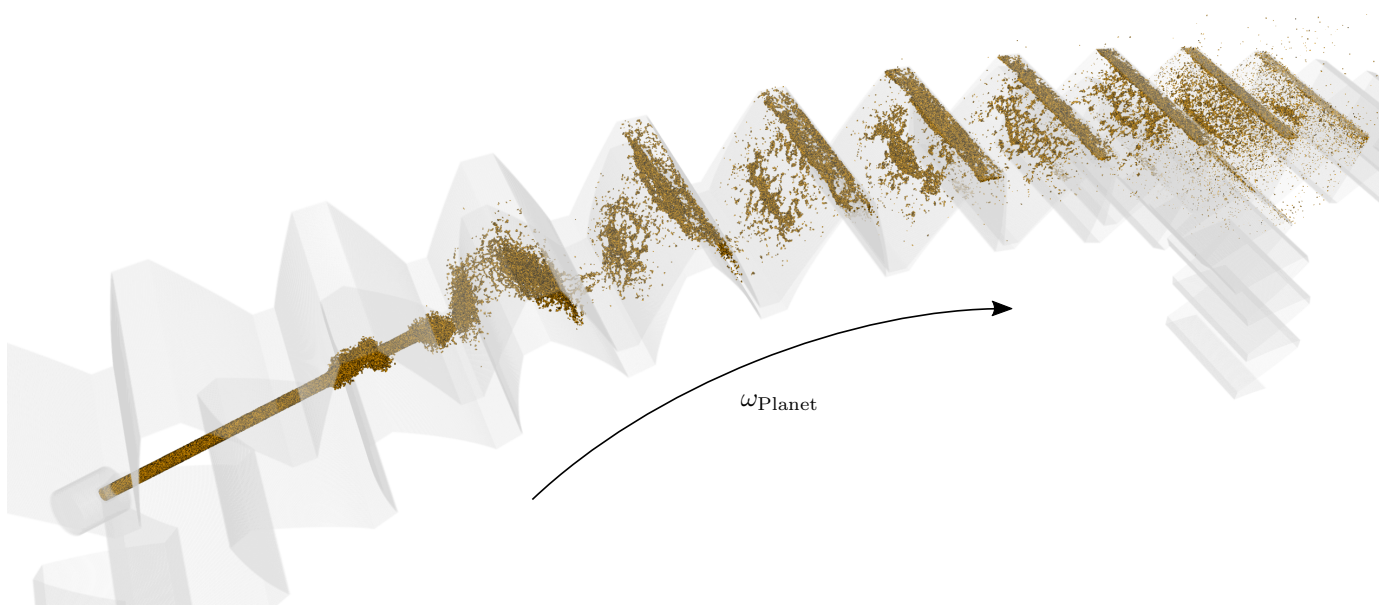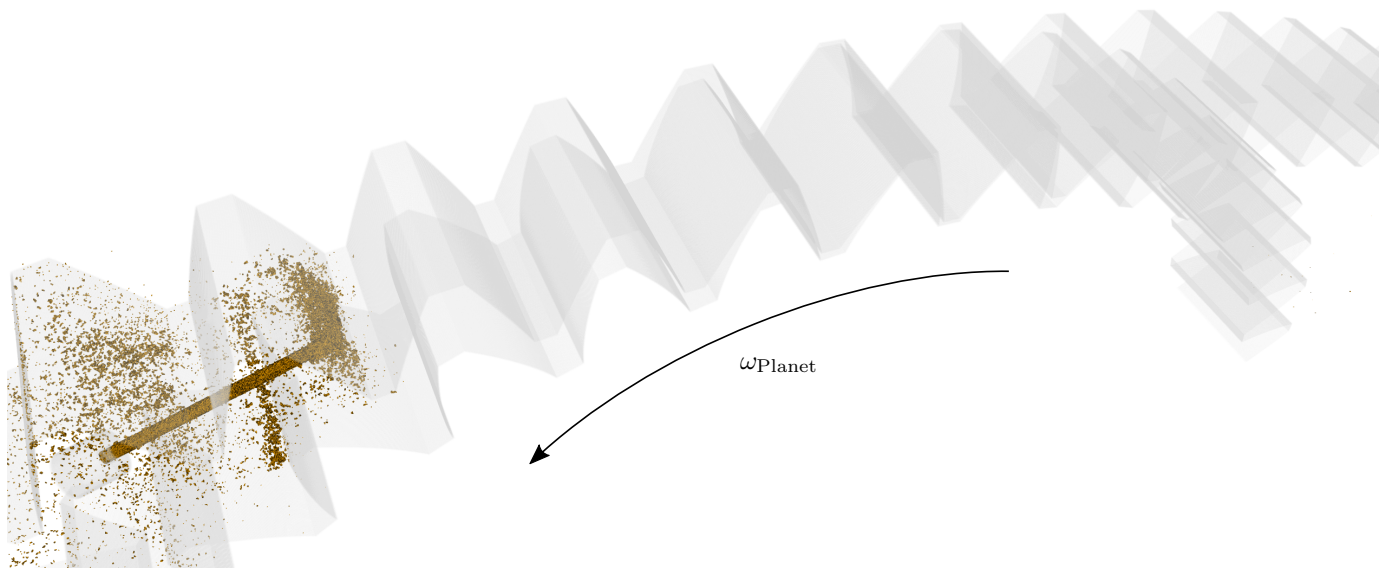
Fig. 6.   3D Oil Distribution (IM)

Fig. 7.   3D Oil Distribution (OOM)

V. Conclusion

In this work the modeling of oil-jet lubrication of an epicyclic gear train was presented. Specifically the interaction of the oil-jet with the gear meshing of the rotating ring gear and a planet gear was investigated. The chosen model was the weakly compressible SPSPH approach with explicit time integration scheme. For the interlocking gears with the heavily deforming computational domain, the Lagrangian SPH framework was an easy choice. Two different nozzle configurations were simulated. The oil-jet was either directed nearly tangential to the gear rotation (IM) or against the gear rotation (OOM) into the meshing. It turned out that the IM configuration is much more promising regarding oil penetration of the meshing compared to OOM configuration. In particular the OOM design turned out to be inferior to the IM design, because all of the oil was ejected before it could reach the meshing.

REFERENCES

[1] L. S. Akin, J. J. Mross, and D. P. Townsend, "Study of lubricant jet flow phenomena in spur gears," Journal of Tribology, vol. 97, no. 2, pp. 283–288, Apr. 1975.

[2] R. F. Handschuh, "Effect of lubricant jet location on spiral bevel gear operating temperatures," NASA, Tech. Rep. NASA/TM—105656, 1992.

[3] Ayan, E., von Plehwe, F. C., Keller, M. C., Kromer, C., Schwitzke, C. und Bauer, H.-J. (2021): Experimental Determination of Heat Transfer Coefficient on Impingement Cooled Gear Flanks: Validation of the Evaluation Method. In: Proceedings of ASME Turbo Expo 2021: Turbomachinery Technical Conference and Exposition, Bd. 5B: Heat Transfer — General Interest; Internal Air Systems; Internal Cooling, id:V05BT13A004, virtuell, online, doi:10.1115/GT2021-58838.

[4] Ayan, E., von Plehwe, F. C., Keller, M. C., Kromer, C., Schwitzke, C. und Bauer, H.-J. (2022): Experimental Determination of Heat Transfer Coefficient on Impingement Cooled Gear Flanks: Validation of the Evaluation Method. Journal of Turbomachinery, Bd. 144(8), id:081008, doi:10.1115/1.4053694.

[5] Untersuchung des Wärmeübergangs durch Einspritzkühlung für ein Höchstleistungsgetriebe. Dissertation, Institut für Thermische Strömungsmaschinen, Karlsruher Institut für Technologie, Karlsruhe, doi:10.30819/5436.

[6] T. Fondelli, A. Andreini, R. Da Soghe, B. Facchini, and L. Cipolla, "Numerical simulation of oil jet lubrication for high speed gears," International Journal of Aerospace Engineering, vol. 2015, no. Article ID 752457, p. 13, 2015.

[7] M. Yazdani and M. C. Soteriou, "A novel approach for modeling the multiscale thermo-fluids of geared systems," International Journal of Heat and Mass Transfer, vol. 72, p. 517–530, 2014.

[8] M. Z. Mettichi, Y. Gargouri, P. H. L. Groenenboom, and F. el Khaldi, "Simulating oil flow for gearbox lubrication using SPH," in Proceedings of the 10th International SPHERIC Workshop, 2015, pp. 237–243.

[9] Keller, M. C., Braun, S., Wieth, L., Chaussonnet, G., Dauch, T., Koch, R., Höfler, C. und Bauer, H.-J. (2016): Numerical Modeling of Oil-Jet Lubrication for Spur Gears using smoothed Particle Hydrodynamics. In: Proceedings of the 11th International SPHERIC Workshop, pp. 69–76, München, doi:10.5445/IR/1000063565.

[10] Keller, M. C., Braun, S., Wieth, L., Chaussonnet, G., Dauch, T. F., Koch, R., Schwitzke, C. und Bauer, H.-J. (2017): Smoothed Particle Hydrodynamics Simulation of Oil-jet Gear Interaction. In: Proceedings of ASME Turbo Expo 2017: Turbomachinery Technical Conference and Exposition, Bd. 2B: Turbomachinery, id:V02BT41A019, Charlotte, North Carolina, USA, doi:10.1115/GT2017-63594.

[11] Keller, M. C., Braun, S., Wieth, L., Chaussonnet, G., Dauch, T. F., Koch, R., Schwitzke, C. und Bauer, H.-J. (2019a): Smoothed Particle Hydrodynamics Simulation of Oil-jet Gear Interaction. Journal of Tribology, Bd. 141(7), id:071703, doi:10.1115/1.4043640.

[12] Keller, M. C., Kromer, C., Cordes, L., Schwitzke, C. und Bauer, H.-J. (2019b): Effect of Design Parameters on Oil-jet Gear Interaction - A CFD Study. In: Proceedings of the 24th ISABE Conference, id:ISABE-2019-24410, Canberra, Australien.

[13] Keller, M. C., Kromer, C., Cordes, L., Schwitzke, C. und Bauer, H.-J. (2020): CFD study of oil-jet gear interaction flow phenomena in spur gears. The Aeronautical Journal, Bd. 124(1279), S.1301–1317, doi:10.1017/aer.2020.44.

[14] M. Keller, "Zur numerischen Simulation der Ölstrahl-Zahnrad-Interaktion in Flugtriebwerken: Eine Studie mit SPH und VOF", 2022, Logos Verlag Berlin, https://doi.org/10.30819/5582.

[15] C. Höfler, S. Braun, R. Koch, and H.-J. Bauer, "Modeling spray formation in gas turbines – a new meshless approach," Journal of Engineering for Gas Turbines and Power, vol. 135, no. 1, pp. 011 503–011 503, Nov. 2012.

[16] S. Braun, M. Krug, L. Wieth, C. Höfler, R. Koch, and H.-J. Bauer, "Simulation of primary atomization: Assessment of the smoothed particle hydrodynamics (SPH) method," in 13th Triennial International Conference on Liquid Atomization and Spray Systems, 2015.

[17] G. Chaussonnet, S. Braun, L. Wieth, R. Koch, H.-J. Bauer, A. Sänger, T. Jakobs, and N. Djordjevic, "SPH simulation of a twin-fluid atomizer operating with a high viscosity liquid," in 13th Triennial International Conference on Liquid Atomization and Spray Systems, 2015.

[18] L. Wieth, C. Lieber, W. Kurz, S. Braun, R. Koch, and H.-J. Bauer, "Numerical modeling of an aero-engine bearing chamber using the meshless smoothed particle hydrodynamics method," in ASME Turbo Expo 2015: Turbine Technical Conference and Exposition, no. GT2015-42316, 2015, p. V02BT39A014.

[19] D. M. Aguirre, M. Okraschevski, N. Bürkle, C. Schwitzke and H.-J. Bauer, "Development of a modelling strategy for cyclic asymmetric problems using the SPH approach", in: Proceedings of the 16th International SPHERIC Workshop, 2022, pp. 55–62, Catania, Italy.

[20] C. Ates, K.V. Muthukumar, M. Okraschevski, N. Bürkle, D. M. Aguirre Bermudez, M. Haber, R. Koch and H.-J. Bauer, "Thin Film Flow Dynamics in Gas-Liquid Contact Reactors", in: Proceedings of the 16th International SPHERIC Workshop, 2022, pp. 55–62, Catania, Italy.

[21] L. Wieth, K. Kelemen, S. Braun, R. Koch, H.-J. Bauer, and H. P. Schuchmann, "Smoothed particle hydrodynamics (SPH) simulation of ahigh-pressure homogenization process," Microfluidics and Nanofluidics, vol. 20, no. 2, pp. 1–18, 2016.

[22] A. Colagrossi and M. Landrini, "Numerical simulation of interfacial flows by smoothed particle hydrodynamics," Journal of Computational Physics, vol. 191, no. 2, pp. 448–475, 2003.

[23] K. Szewc, J. Pozorski, and J.-P. Minier, "Analysis of the incompressibility constraint in the smoothed particle hydrodynamics method," International Journal for Numerical Methods in Engineering, vol. 92, no. 4, pp. 343–369, 2012.

[24] Adami, S., Hu, X., and Adams, N., 2010. "A new surface- tension formulation for multi-phase SPH using a reproduc- ing divergence approximation". Journal of Computational Physics, 229(13), pp. 5011–5021.

[25] Wieth, L., Braun, S., Koch, R., and Bauer, H.-J., 2014. "Modeling of liquid-wall interaction using the smoothed particle hydrodynamics (SPH) method". In ILASS Europe, 26th Annual Conference on Liquid Atomization and Spray Systems.

[26] DIN ISO 21771: 2014-08, "Gears - Cylindrical involute gears and gear pairs - Concepts and geometry (ISO 21771:2007)", https://dx.doi.org/10.31030/2144663

[27] Shepard, D.: A Two-dimensional Interpolation Function for Irregularly-spaced Data. In: Proceedings of the 1968 23rd ACM National Conference, pp 517–524, Princeton, New Jersey, USA, doi:10.1145/800186.810616.

[28] Randles, P. W. und Libersky, L. D.: Smoothed Particle Hydrodynamics: Some recent improvements and applications. Computer Methods in Applied Mechanics and Engineering, Bd. 139(1–4), pp. 375–408, doi:10.1016/s0045-7825(96)01090-0.

[29] S. Braun, L. Wieth, R. Koch, and H.-J. Bauer, "A framework for permeable boundary conditions in SPH: inlet, outlet, periodicity," in Proceedings of the 10th International SPHERIC Workshop, 2015, pp. 237–243.